Electronic Supplementary Material (ESI) for Soft Matter.

SUPPORTING INFORMATION

Artificial Light-Harvesting Systems Based on Supramolecular Self-Assembly Multi-Component Metallogels

Xinxian Ma*, Yipei Wang#, Yingshan Lai, Tianqi Ren, Jiahong Tang, Yang Gao, Yutao Geng, Jiali Zhang

College of Chemistry and Chemical Engineering, Ningxia Normal University, Guyuan 756000, People's Republic of China. Fax: 86 954 2079637; Tel: 86 954 2079637; E-mail: maxinxian@163.com

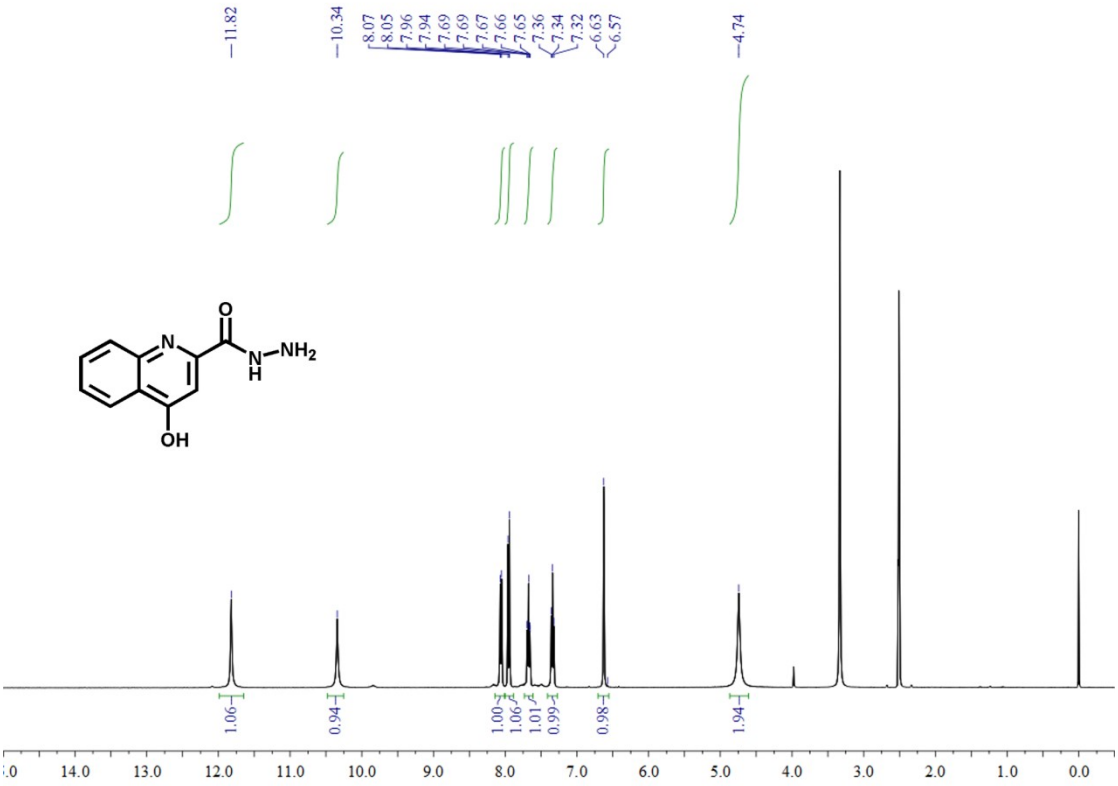

Fig. S1. ^{1}H NMR spectrum of **L1** in DMSO-d_6

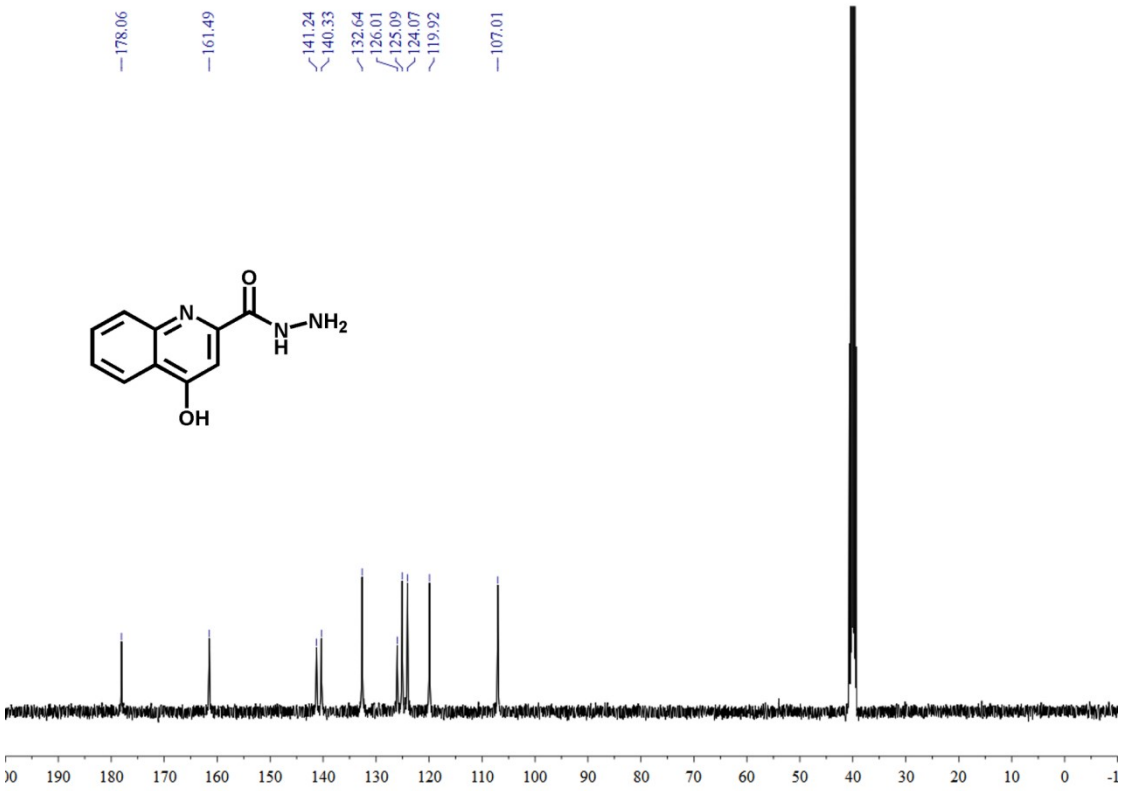

Fig. S2. ^{13}C NMR spectrum of **L1** in DMSO-d_6

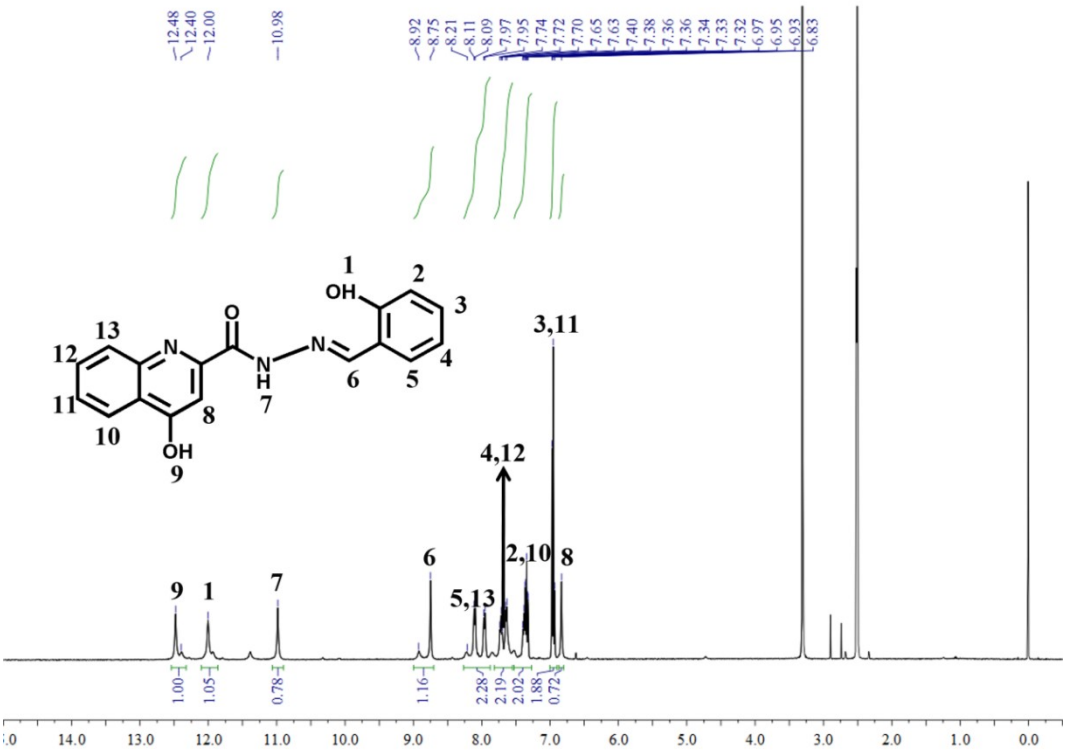

Fig. S3. ^{1}H NMR spectrum of **L** in DMSO-d_6

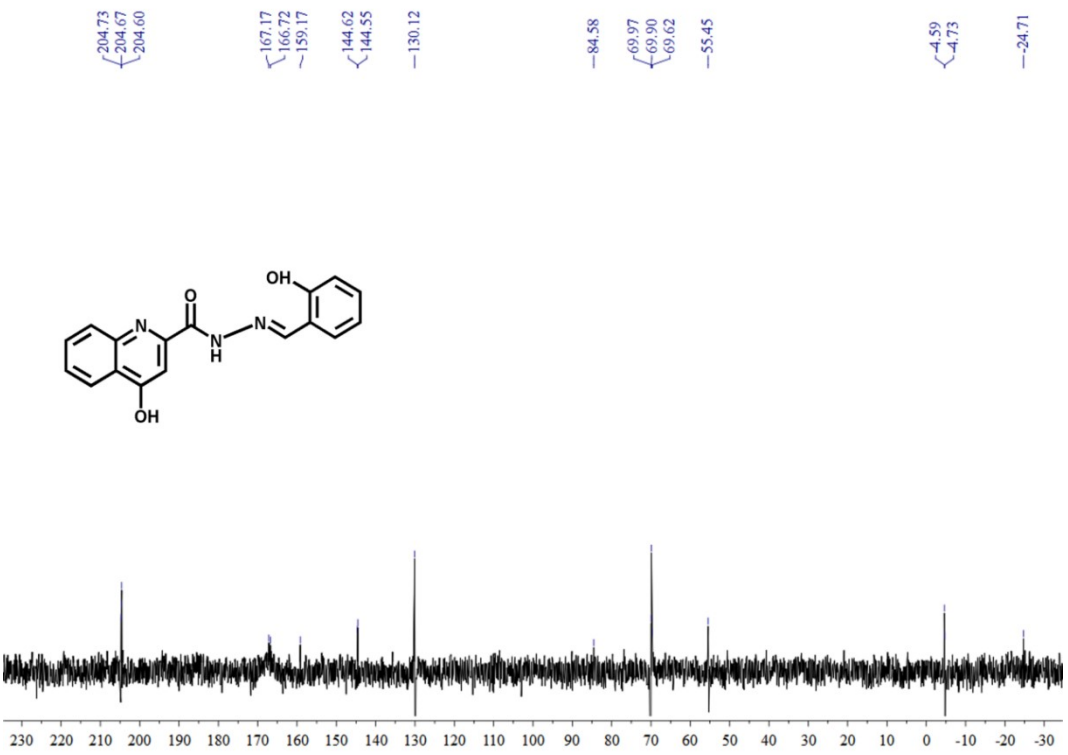

Fig. S4. ^{13}C NMR spectrum of **L** in DMSO-d_6

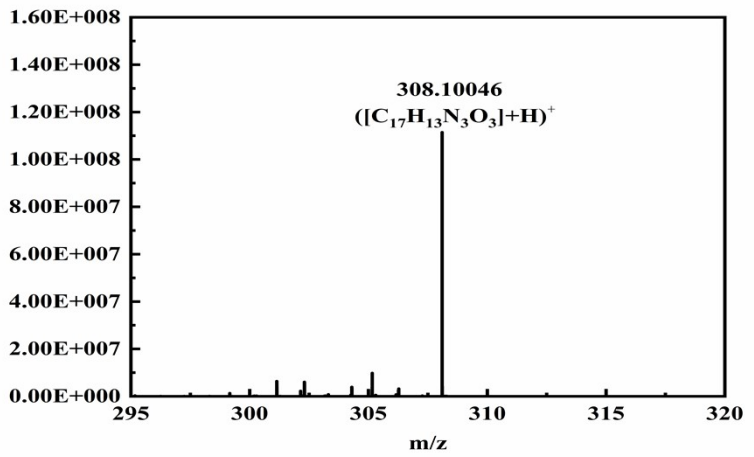

Fig. S5. ESI-MS spectrum of **L**

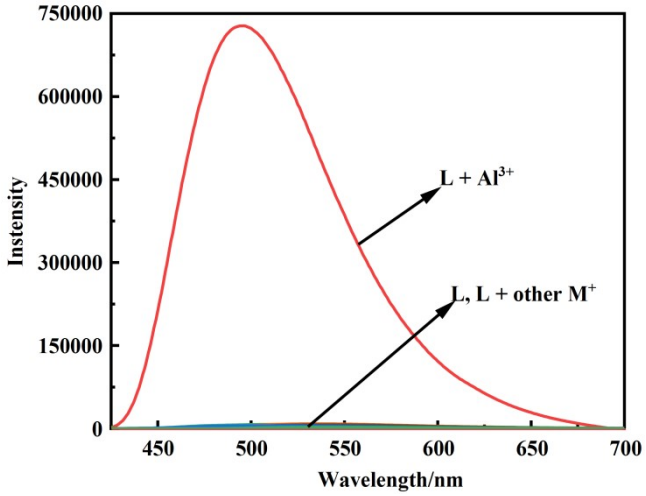

Fig. S6. Luminescence spectra of L (1×10^{-3} mol·L^{-1}) in DMSO with different metal cations (Al^{3+}, Zn^{2+}, Ag^{+}, Hg^{2+}, Mn^{2+}, Na^{+}, Cr^{3+}, K^{+}, Cd^{2+}, Fe^{3+}, Ni^{2+}, Cu^{2+}, Mg^{2+}, Pb^{2+} and Co^{2+} (2.0 equiv, 0.1 mol·L^{-1}) λ_{ex} = 411 nm).

Table S1 Gelation properties of the L

Entry	Solvent	State[a]	CGC[b](%)	T_{gel}[c] (℃, wt %)
1	water	P	\	\
2	cyclohexane	P	\	\
3	petroleum ether	P	\	\
4	THF	P	\	\
5	$CHCl_3$	P	\	\
6	CH_2Cl_2	P	\	\
7	acetone	P	\	\
8	DMF	S	\	\
9	DMF-H_2O	P	\	\
10	DMSO	S	\	\
11	DMSO-H_2O	P	\	\
12	methanol	P	\	\
13	ethanol	P	\	\
14	ethanol-H_2O	P	\	\
15	ethanediol	P	\	\
16	isopropanol	P	\	\
17	n-butyl alcohol	P	\	\
18	n-amyl alcohol	P	\	\
19	isopentanol	P	\	\
20	n-hexanol	P	\	\
21	ethyl acetate	P	\	\
22	acetonitrile	P	\	\
23	CCl_4	P	\	\
24	B-DMSO-H_2O	G	0 ~ 0.04 g/mL DMSO[d]	84 (± 0.5) ℃[e]

a G, P and S denote gelation, precipitation and solution, respectively
b The critical gelation concentration (wt %, 10 mg/mL = 1.0%)
c The gel-sol transition temperature (℃)
d L within the solubility of DMSO, the gel can be successfully prepared.
e 0.015 g L, V_{BD} : V_D : V_{water} = 1 : 1 : 2

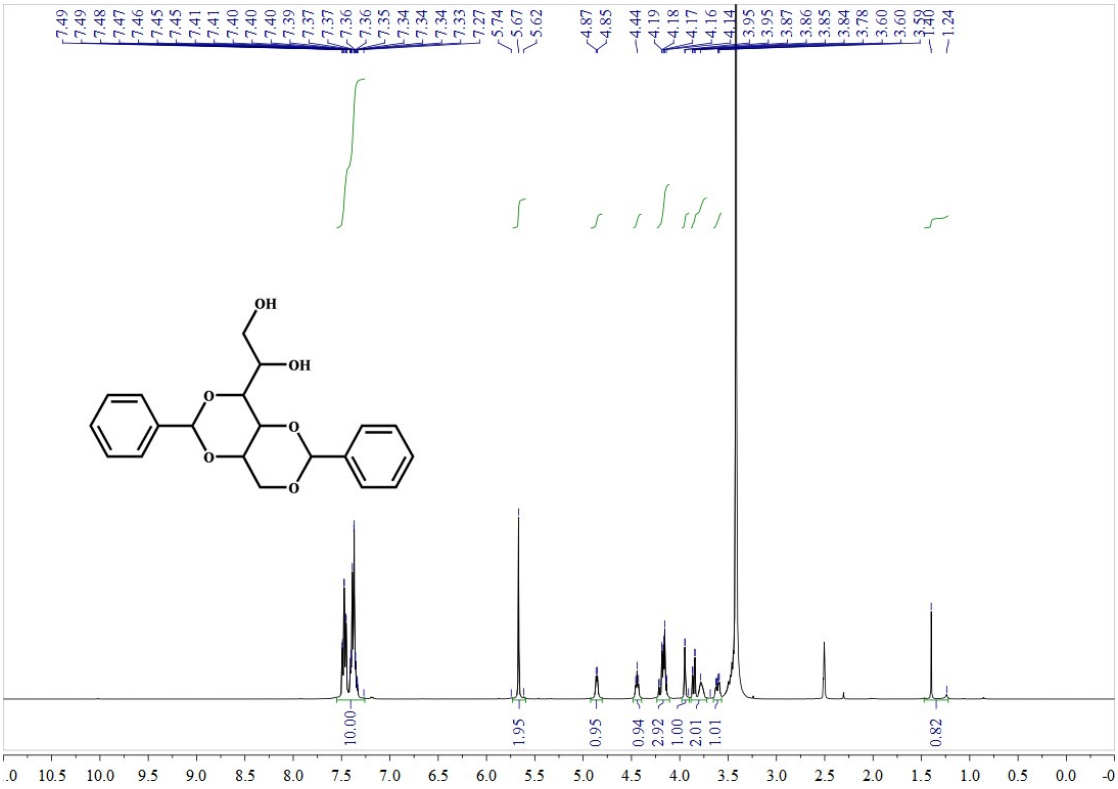

Fig. S7. ^{1}H NMR spectrum of **B** in DMSO-d_6.

Fig. S8. Illustration for reversible gel-liquid transformation of the L-B-gel triggered by temperature (0.015 g L, 0.1 mol·L^{-1} B in DMSO, V_{BD} : V_D : V_{water} = 1 : 1 : 2).

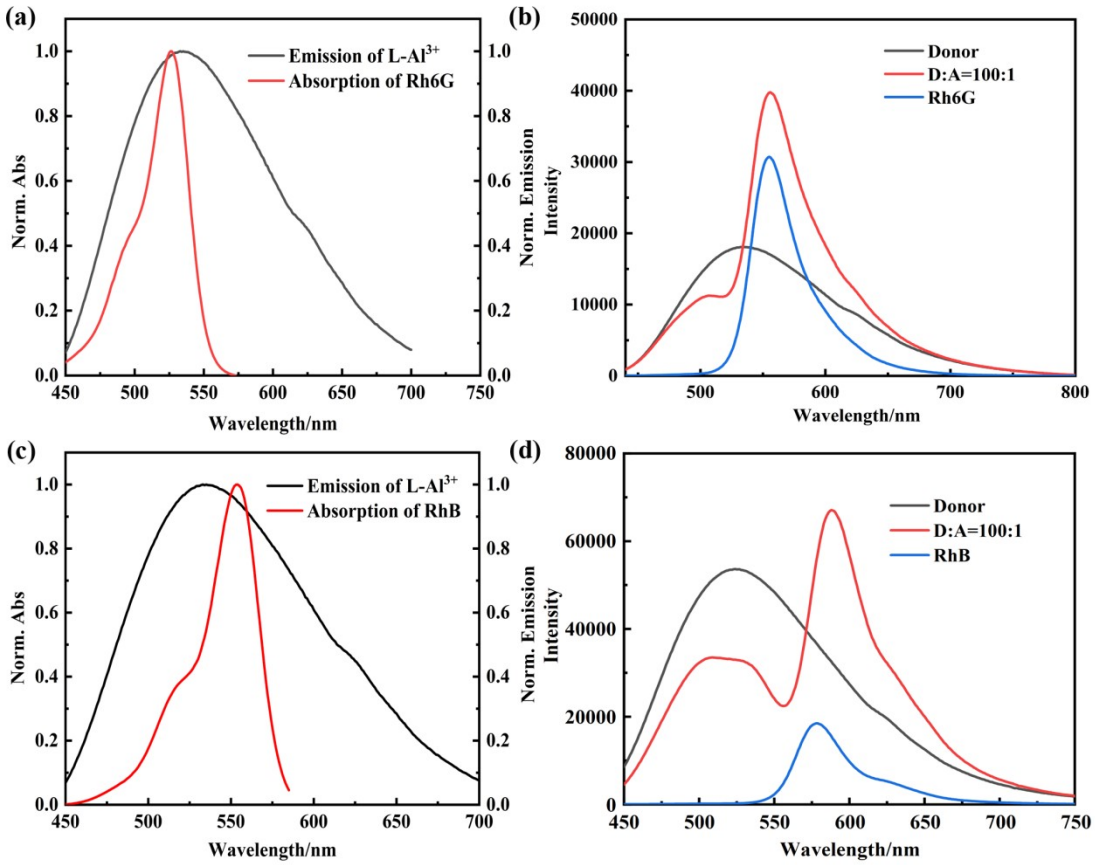

Fig. S9. (a) Normalized emission spectrum of L-Al^{3+} (λ_{ex} = 427 nm, [L-Al^{3+}] = 3 × 10^{-6} M), absorption spectrum of Rh6G ([Rh6G] = 10^{-5} mol·L^{-1}). (b) Fluorescence contrast spectra of L-Al^{3+}/Rh6G and pure Rh6G in the same proportion (100 : 1, [L-Al^{3+}] = 1.5 × 10^{-6} M, [Rh6G] = 1.5 × 10^{-8} M, λ_{ex} = 427 nm). (c) Normalized emission spectrum of L-Al^{3+} (λ_{ex} = 427 nm, [L-Al^{3+}] = 3 × 10^{-6} M), absorption spectrum of RhB ([RhB] = 5 × 10^{-5} mol·L^{-1}). (d) Fluorescence contrast spectra of L-Al^{3+}/RhB and pure RhB in the same proportion (100 : 1, [L-Al^{3+}] = 1.5 × 10^{-6} M, [RhB] = 1.5 × 10^{-8} M, λ_{ex} = 427 nm). All experiments were carried out in DMSO solution.

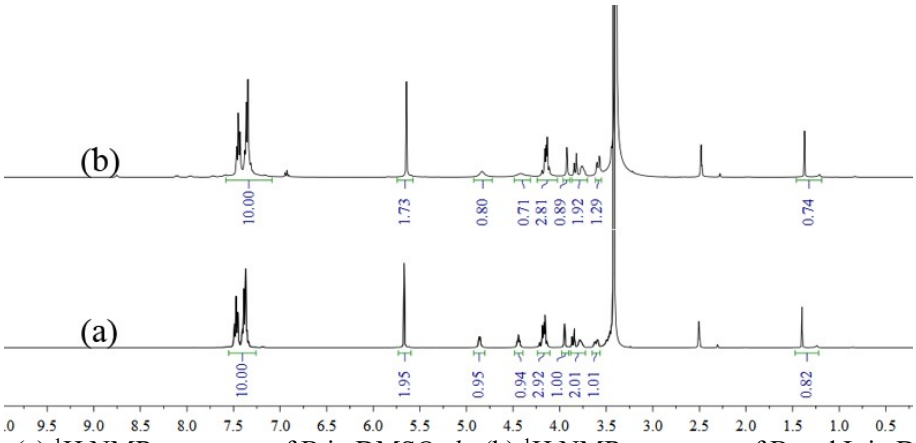

Fig. S10. (a) ^{1}H NMR spectrum of B in DMSO-d_6. (b) ^{1}H NMR spectrum of B and L in DMSO-d_6.

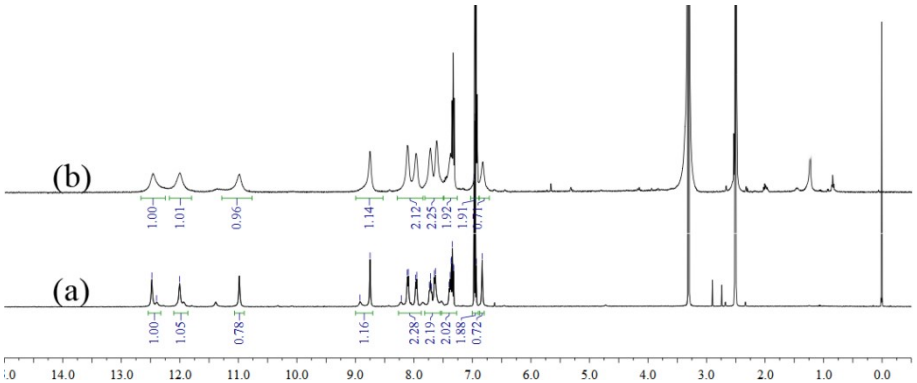

Fig. S11. (a) ^{1}H NMR spectrum of L in DMSO-d_6. (b) ^{1}H NMR spectrum of L-B-gel in DMSO-d_6.

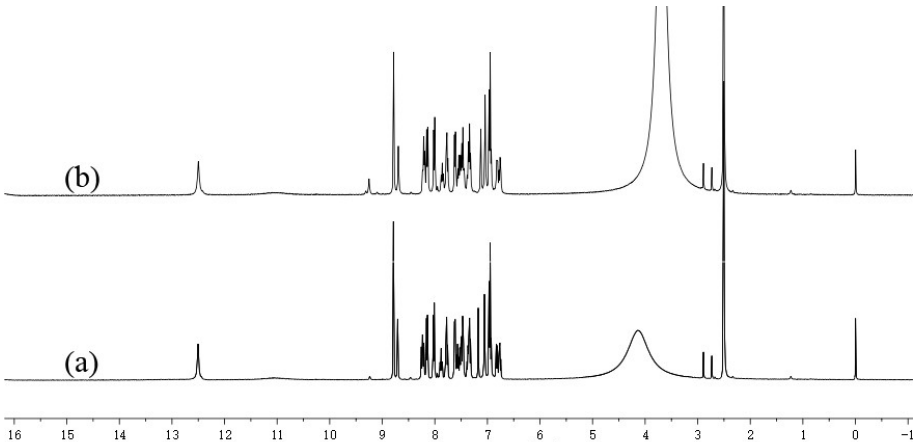

Fig. S12. (a) ^{1}H NMR spectrum of L-Al^{3+} in DMSO-d_6. (b) ^{1}H NMR spectrum of L-Al^{3+}-B-gel in DMSO-d_6.

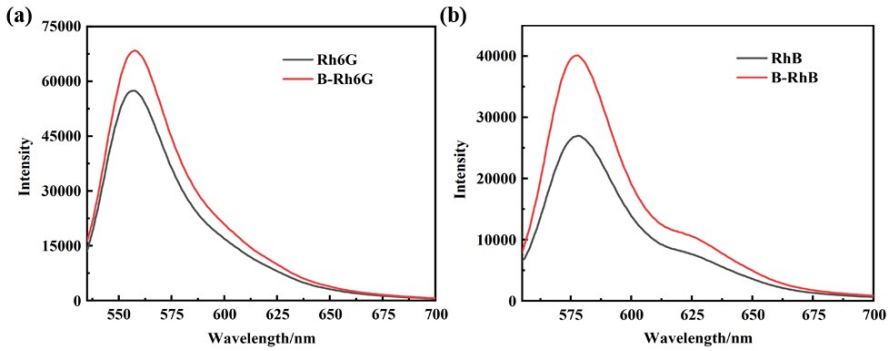

Fig. S13. (a) Fluorescence contrast spectra of Rh6G and B-Rh6G. (b) Fluorescence contrast spectra of RhB and B-RhB.

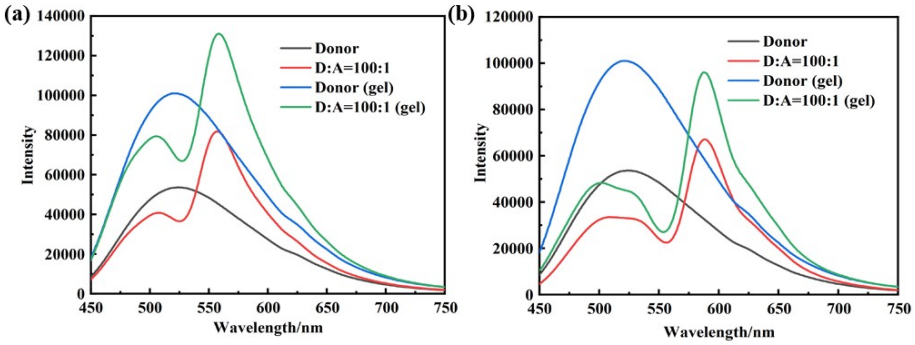

Fig. S14. (a) Fluorescence contrast spectra of solution state and gel state (Rh6G). (b) Fluorescence contrast spectra of solution state and gel state (RhB).

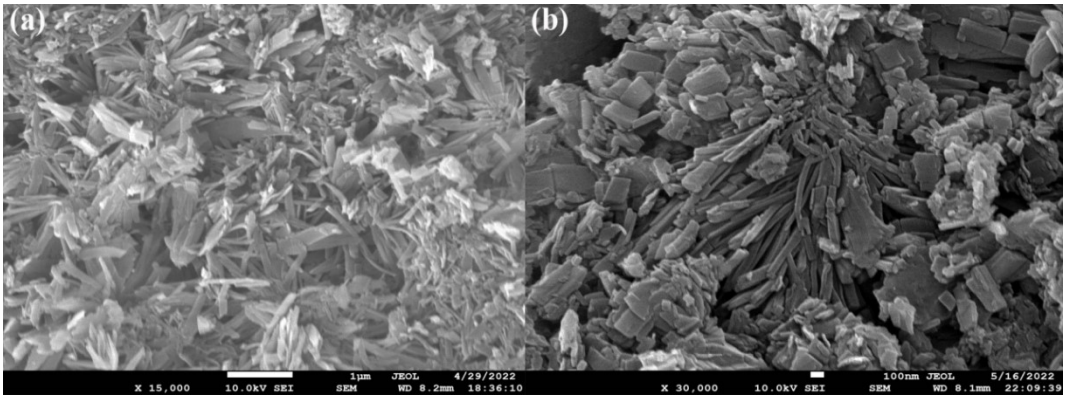

Fig. S15. (a) The SEM image of as-prepared L-Al^{3+}-B/Rh6G-gel in mixed solution at room temperature (L : Al^{3+} = 1 : 1, n : n; V_{BD} : V_D : V_{water} = 1 : 1 : 2). (b) The SEM image of as-prepared L-Al^{3+}-B/RhB-gel in mixed solution at room temperature (L : Al^{3+} = 1 : 1, n : n; V_{BD} : V_D : V_{water} = 1 : 1 : 2).

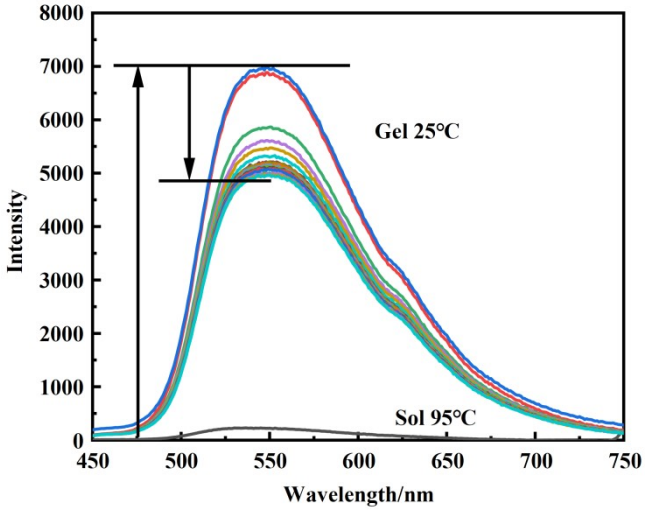

Fig. S16. Temperature-dependent fluorescent spectra of L-B-gel (V_{BD} : V_D : V_{water} = 1 : 1 : 2, 0.02 g L, 0.1 mol·L^{-1} B in DMSO) during the gelation process (λ_{ex} = 378 nm).

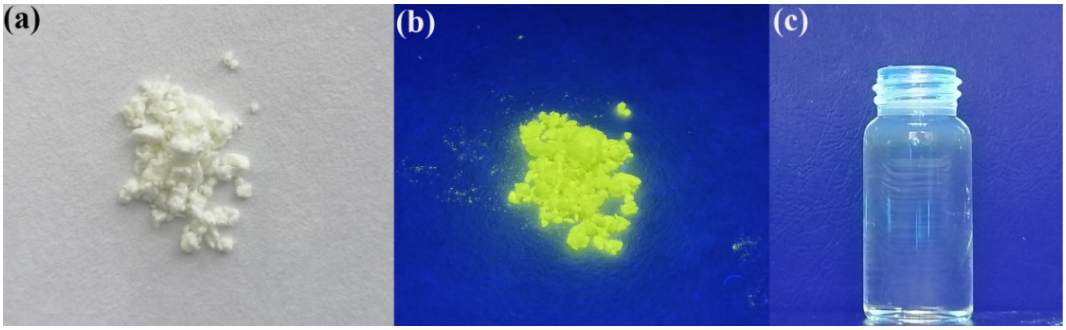

Fig. S17. The photos of L powder (25 ℃) were taken under (a) daylight and (b) UV light, respectively. (c) The photo of L in DMSO (5×10^{-5} M, 25℃) was taken under UV light.

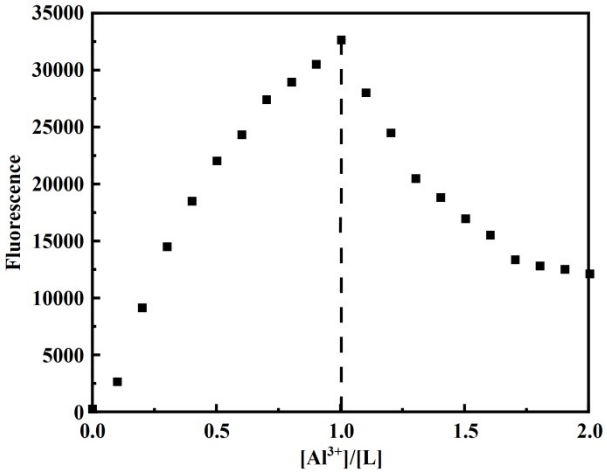

Fig. S18. Job's plots according to the way for continuous variations, indicating the 1 : 1 stoichiometry for L-Al^{3+} (λ_{ex} = 428 nm, The concentrations of L and Al^{3+} are 1 × 10^{-3} mol·L^{-1}).

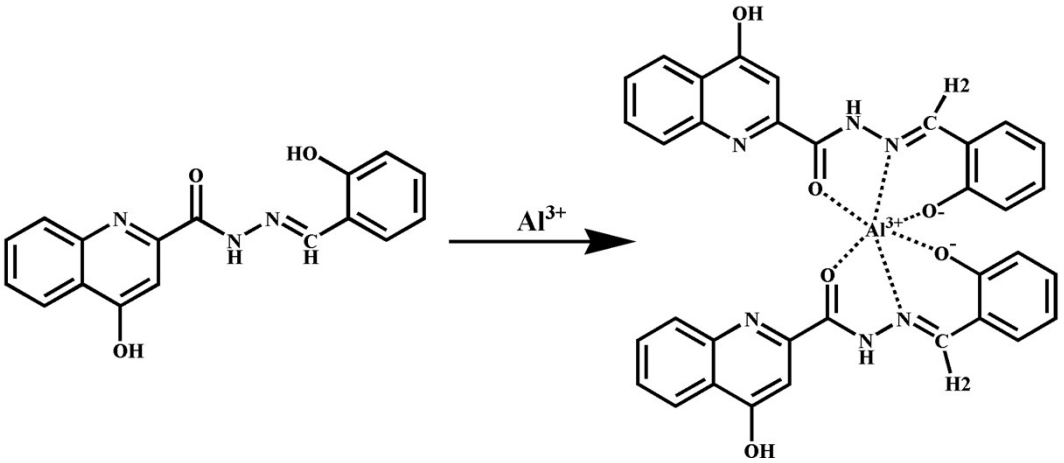

Fig. S19. Possible coordination mechanism of L for Al^{3+}.

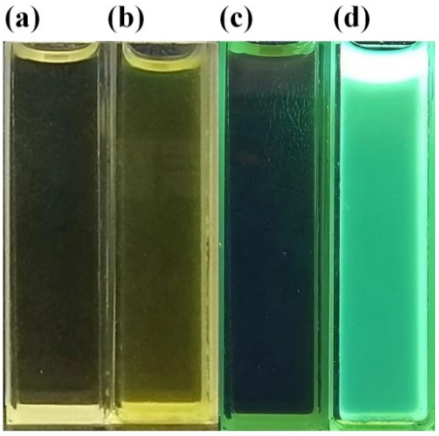

Fig. S20. Photographs of (a) L (4.5×10^{-6} M) and (b) L-Al^{3+} ([L] = 4.5×10^{-6} M, [Al^{3+}] = 4.5×10^{-6} M) under natural light irradiation. Photographs of (c) L (4.5×10^{-6} M) and (d) L-Al^{3+} ([L] = 4.5×10^{-6} M, [Al^{3+}] = 4.5×10^{-6} M) under UV lamp irradiation.

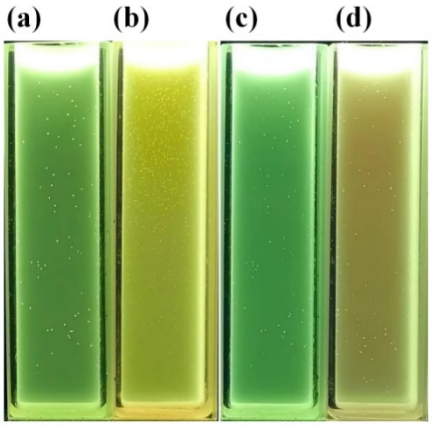

Fig. S21. Photographs of (a) L-Al^{3+} (2×10^{-6} M) and (b) L-Al^{3+}/Rh6G ([L-Al^{3+}] = 2×10^{-6} M, [Rh6G] = 2×10^{-8} M) in DMF under UV lamp irradiation. Photographs of (c) L-Al^{3+} (2×10^{-6} M) and (d) L-Al^{3+}/RhB ([L-Al^{3+}] = 2×10^{-6} M, [RhB] = 2×10^{-8} M) in DMF under UV lamp irradiation.

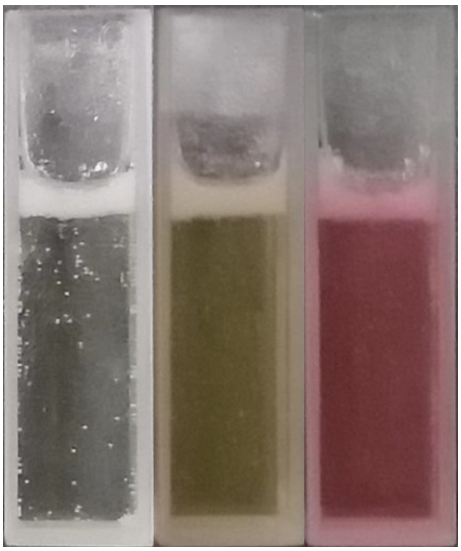

Fig. S22. Pictures of L-Al^{3+}, L-Al^{3+}/Rh6G and L-Al^{3+}/RhB under natural light from left to right (DMSO solution).

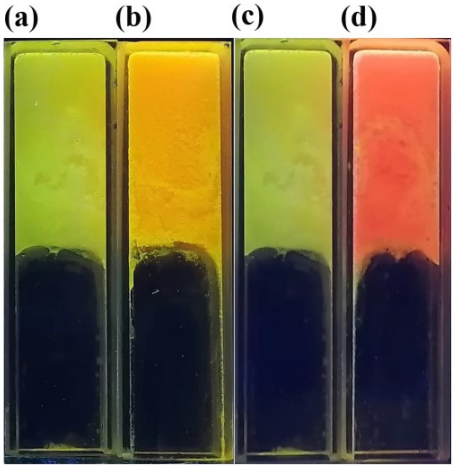

Fig. S23. Photographs of (a) L-Al^{3+}-B-gel ([L-Al^{3+}] = 5 × 10^{-5} M) and (b) L-Al^{3+}-B/Rh6G-gel ([L-Al^{3+}] = 5 × 10^{-5} M, [Rh6G] = 5 × 10^{-7} M, V_{BD} : V_D : V_{water} = 1 : 1 : 2) under UV lamp irradiation. Photographs of (c) L-Al^{3+}-B-gel ([L-Al^{3+}] = 5 × 10^{-5} M) and (d) L-Al^{3+}-B/RhB-gel ([L-Al^{3+}] = 5 × 10^{-5} M, [RhB] = 5 × 10^{-7} M, V_{BD} : V_D : V_{water} = 1 : 1 : 2) under UV lamp irradiation.

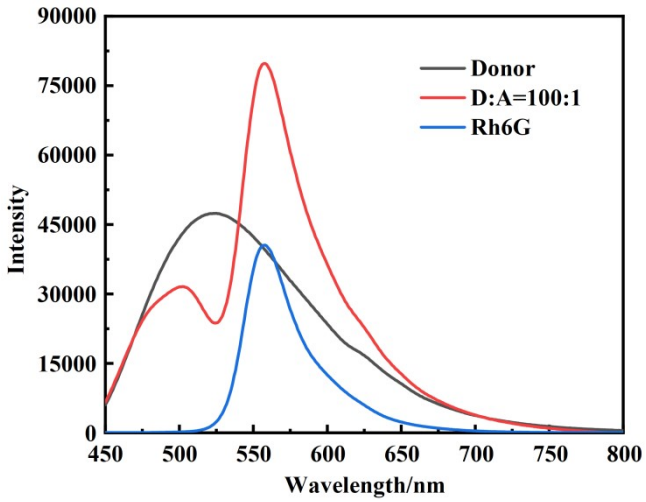

Fig. S24. Fluorescence contrast spectra of L-Al^{3+}/Rh6G and pure Rh6G in the same proportion (100 : 1, [L-Al^{3+}] = 1.5 × 10^{-6} M, [Rh6G] = 1.5 × 10^{-8} M, and λ_{ex} = 437 nm).

Energy-transfer efficiency (Φ_{ET}) was calculated from spectra using equation S1.

$$\Phi_{ET} = 1\text{-}I_{DA}/I_D \text{ (eq. S1)}^1$$

Where I_{DA} and I_D are the fluorescence intensities of the excitation of L-Al^{3+}/Rh6G assembly (donor and acceptor) and L-Al^{3+} assembly (donor), respectively at 437 nm.

The Φ_{ET} was calculated as 33.40% in solvent, measured under the condition of [L-Al^{3+}] = 1.5 × 10^{-6} M, [Rh6G] = 1.5 × 10^{-8} M, and λ_{ex} = 437 nm.

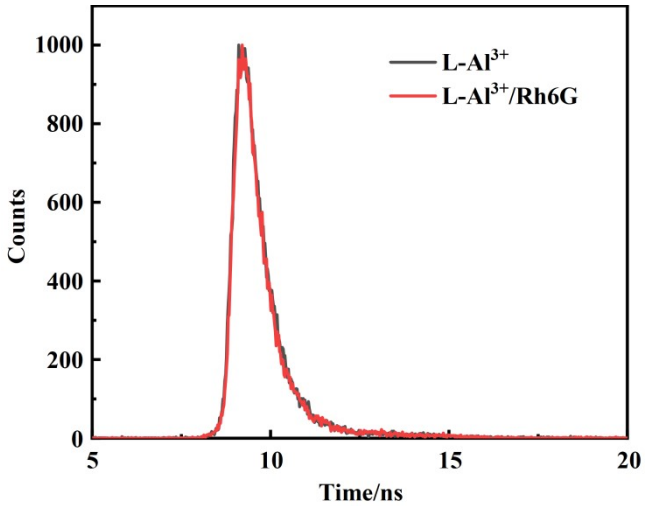

Fig. S25. Fluorescence decay profiles of L-Al^{3+} assembly (black line, [L-Al^{3+}] = 1.5 × 10^{-6} M, Monitored at 502 nm upon excitation at 437 nm) and L-Al^{3+}/Rh6G assembly (red line, [L-Al^{3+}] = 1.5 × 10^{-6} M, [Rh6G] = 1.5 × 10^{-8} M, Monitored at 502 nm upon excitation at 437 nm).

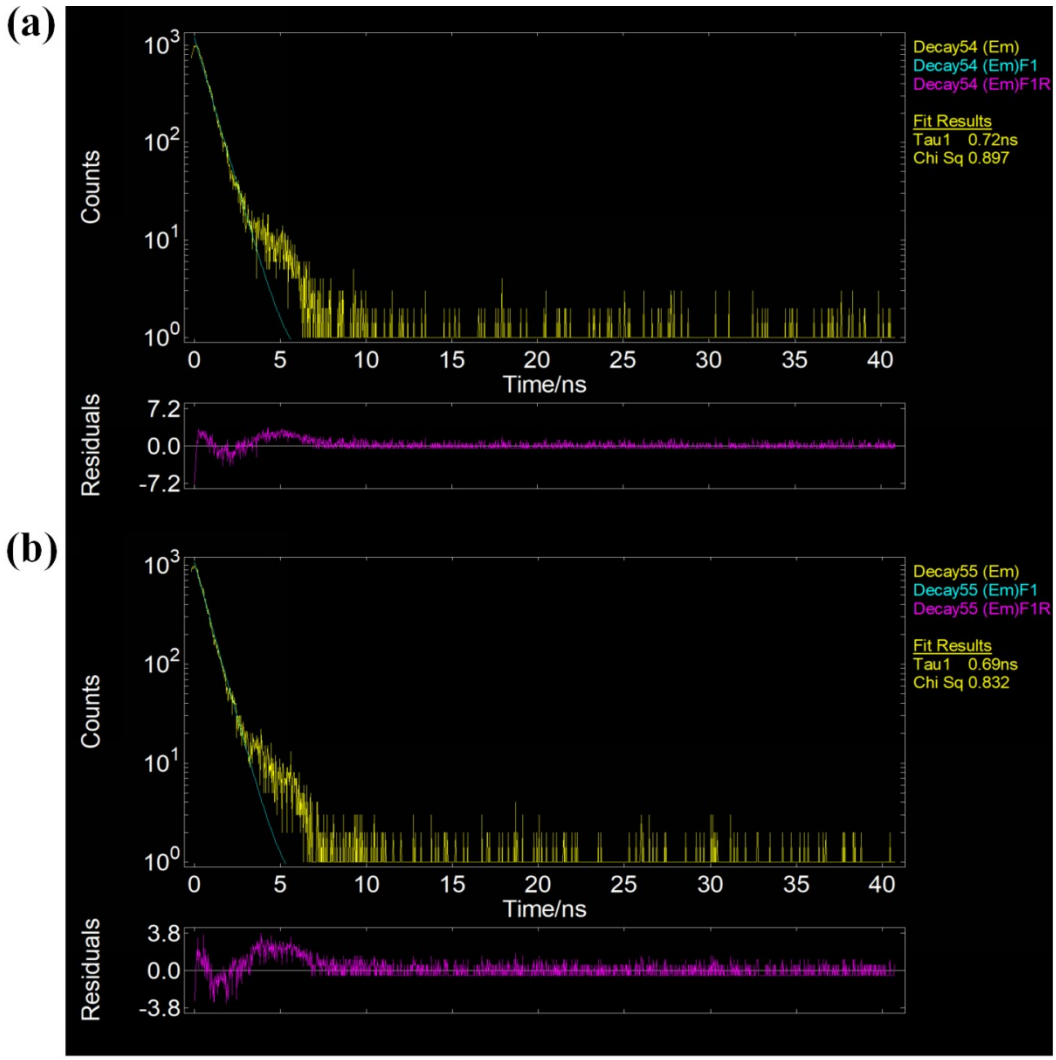

Fig. S26. (a) Fluorescence lifetime of L-Al^{3+} ([L-Al^{3+}] = 1.5 × 10^{-6} M. Monitored at 502 nm upon excitation at 437 nm). (b) Fluorescence lifetime of L-Al^{3+}/Rh6G ([L-Al^{3+}] = 1.5 × 10^{-6} M, [Rh6G] = 1.5 × 10^{-8} M. Monitored at 502 nm upon excitation at 437 nm.)

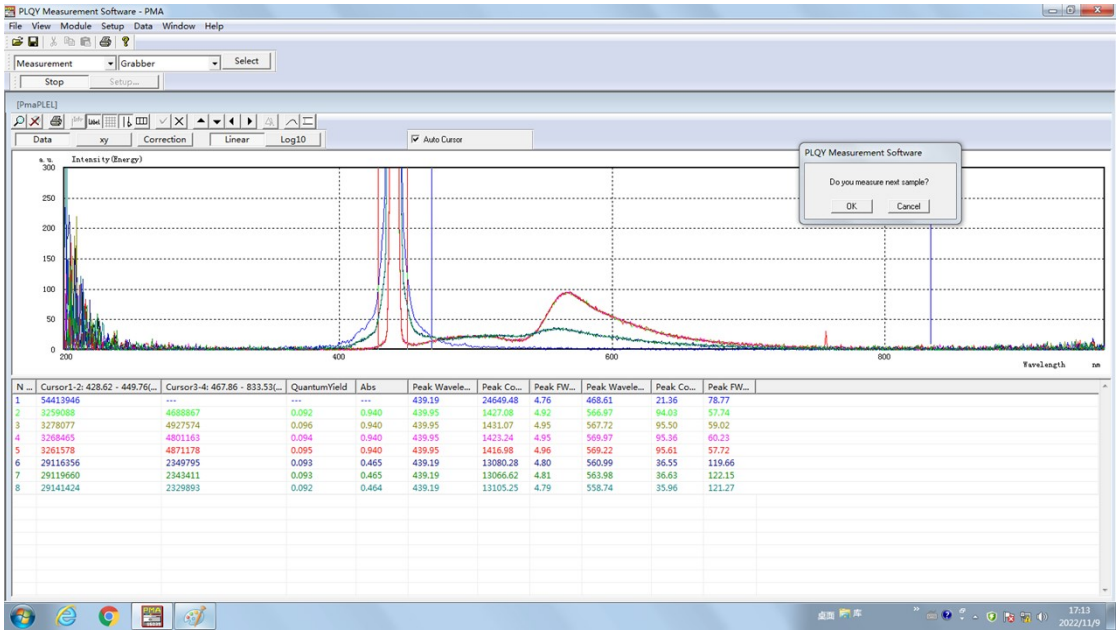

N ...	Cursor1-2: 428.62 - 449.76(...	Cursor3-4: 467.86 - 833.53(...	QuantumYield	Abs	Peak Wavele...	Peak Co...	Peak FW...	Peak Wavele...	Peak Co...	Peak FW...
1	54413946	---	---	---	439.19	24649.48	4.76	468.61	21.36	78.77
2	3259088	4688867	0.092	0.940	439.95	1427.08	4.92	566.97	94.03	57.74
3	3278077	4927574	0.096	0.940	439.95	1431.07	4.95	567.72	95.50	59.02
4	3268465	4801163	0.094	0.940	439.95	1423.24	4.95	569.97	95.36	60.23
5	3261578	4871178	0.095	0.940	439.95	1416.98	4.96	569.22	95.61	57.72
6	29116356	2349795	0.093	0.465	439.19	13080.28	4.80	560.99	36.55	119.66
7	29119660	2343411	0.093	0.465	439.19	13066.62	4.81	563.98	36.63	122.15
8	29141424	2329893	0.092	0.464	439.19	13105.25	4.79	558.74	35.96	121.27

Fig. S27. Quantum yield diagram of L-Al^{3+}/Rh6G assembly with luminescence range of 520-750 nm ([L-Al^{3+}] = 1.5 × 10^{-6} M, [Rh6G] = 1.5 × 10^{-8} M).

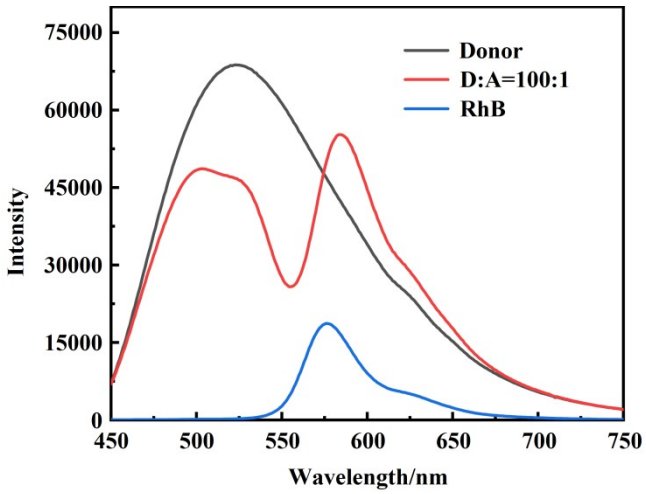

Fig. S28. Fluorescence contrast spectra of L-Al^{3+}/RhB and pure RhB in the same proportion (100 : 1, [L-Al^{3+}] = 1.5 × 10^{-6} M, [RhB] = 1.5 × 10^{-8} M, λ_{ex} = 437 nm).

Φ_{ET} was calculated from spectra using equation S1.

$$\Phi_{ET} = 1\text{-}I_{DA}/I_D \text{ (eq. S1)}^1$$

Where I_{DA} and I_D are the fluorescence intensities of the excitation of L-Al^{3+}/RhB assembly (donor and acceptor) and L-Al^{3+} assembly (donor), respectively at 437 nm.

The Φ_{ET} was calculated as 30.16% in solvent, measured under the condition of [L-Al^{3+}] = 1.5 × 10^{-6} M, [RhB] = 1.5 × 10^{-8} M, and λ_{ex} = 437 nm.

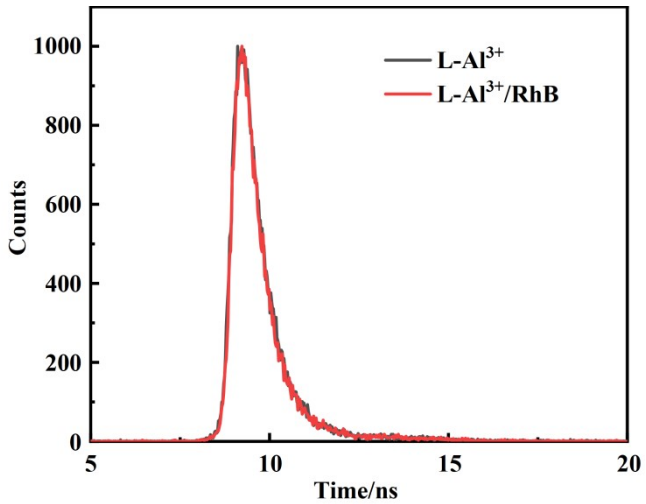

Fig. S29. Fluorescence decay profiles of L-Al^{3+} assembly (black line, [L-Al^{3+}] = 1.5 × 10^{-6} M. Monitored at 502 nm upon excitation at 437 nm), and L-Al^{3+}/RhB assembly (red line, [L-Al^{3+}] = 1.5 × 10^{-6} M, [RhB] = 1.5 × 10^{-8} M. Monitored at 502 nm upon excitation at 437 nm).

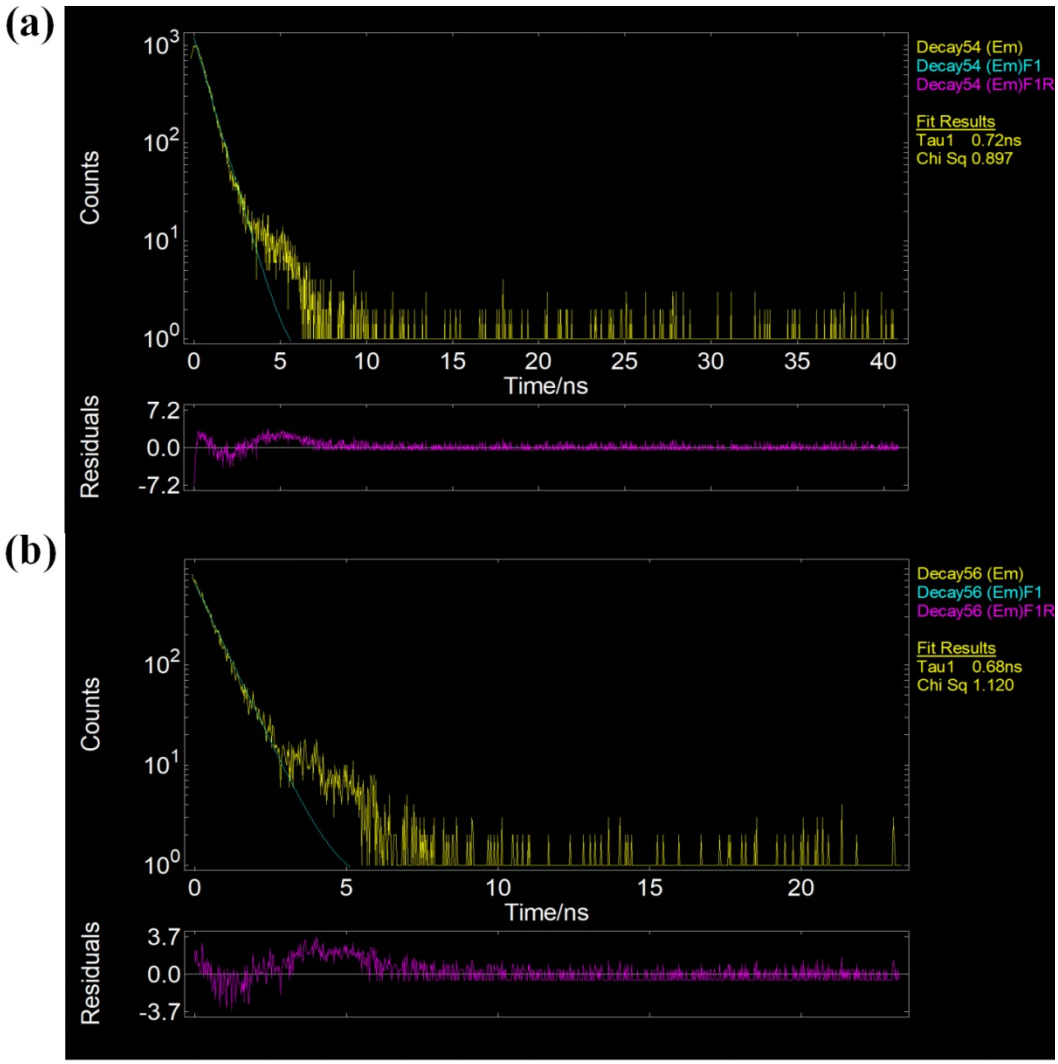

Fig. S30. (a) Fluorescence lifetime of L-Al^{3+} ([L-Al^{3+}] = 1.5 × 10^{-6} M. Monitored at 502 nm upon excitation at 437 nm). (b) Fluorescence lifetime of L-Al^{3+}/RhB ([L-Al^{3+}] = 1.5 × 10^{-6} M, [RhB] = 1.5 × 10^{-8} M. Monitored at 502 nm upon excitation at 437 nm.)

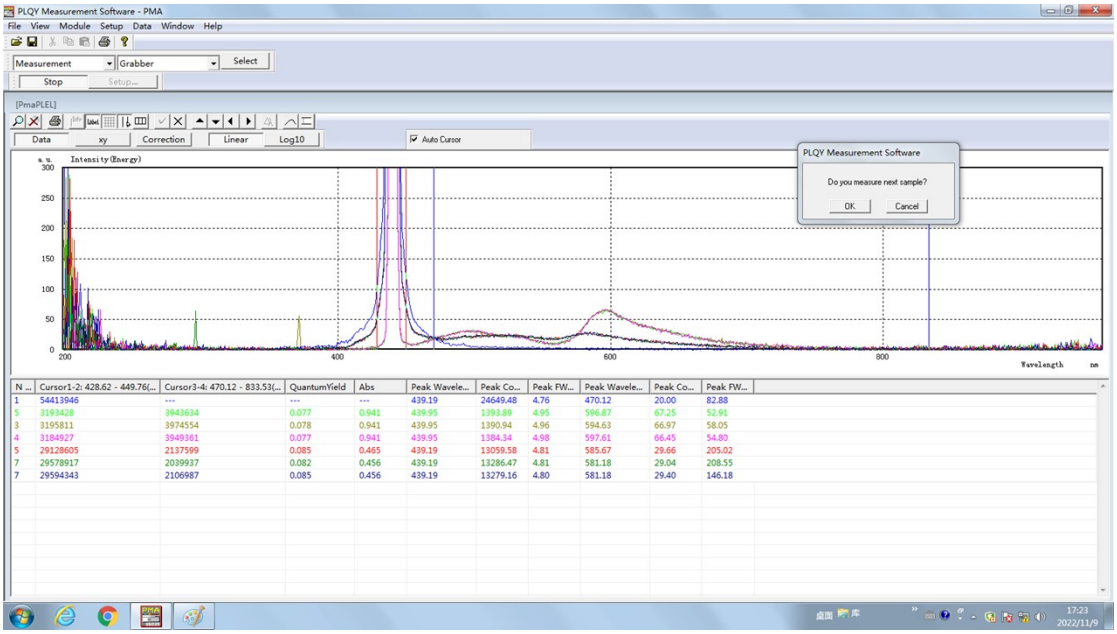

Fig. S31. Quantum yield diagram of L-Al^{3+}/RhB assembly with luminescence range of 550-750 nm. ([L-Al^{3+}] = 1.5×10^{-6} M, [RhB] = 1.5×10^{-8} M)

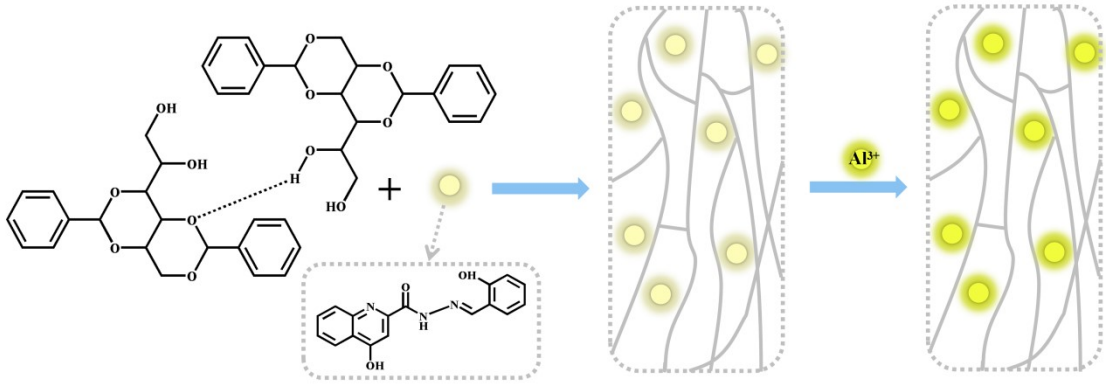

Fig. S32. Possible formation mechanism of L-Al^{3+}-B-gel.[2]

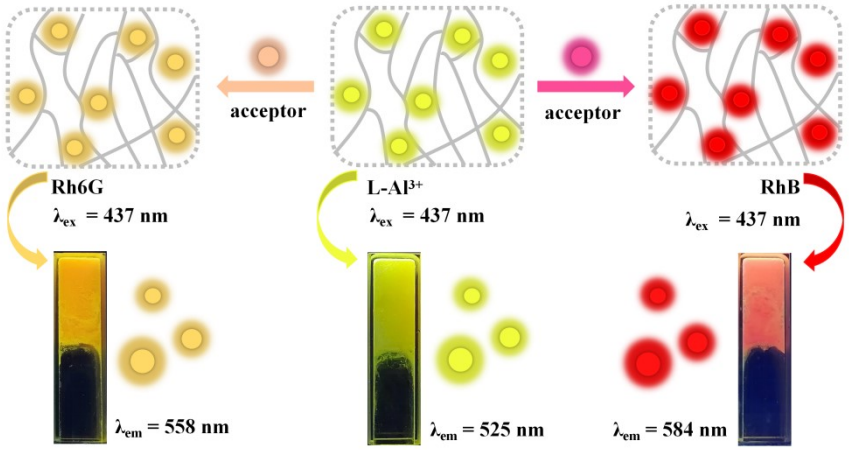

Fig. S33. Possible mechanism of light-harvesting systems.

1. (a) S. Guo, Y. Song, Y. He, X. Y. Hu, L. Y. Wang, Highly Efficient Artificial Light-Harvesting Systems Constructed in Aqueous Solution Based on Supramolecular Self-Assembly, Angew. Chem. Int. Ed. 2018, 57, 3163-3167. (b) M. Hao, G. P. Sun, M. Z. Zuo, Z. Q. Xu, Y. Chen, X. Y. Hu, L. Y. Wang, Highly efficient artificial light-harvesting system with two-step sequential energy transfer based on supramolecular self-assembly, Angew. Chem. Int. Ed. 2020, 59, 10095-10100.

2. (a) W. C. Lai, Y. C. Lee, Self-assembly behavior of gels composed of dibenzylidene sorbitol derivatives and poly (ethylene glycol), RSC Adv., 2016, 6, 98042-98051. (b) W. C. Lai, S. C. Tseng, Novel polymeric nanocomposites and porous materials prepared using organogels, Nanotechnology., 2009, 20, 475606. (c) C. Lai, S. C. Tseng, S. H. Tung, Y. E. Huang, S. Raghavan, Nanostructured Polymers Prepared Using a Self-Assembled Nanofibrillar Scaffold as a Reverse Template, J. Phys. Chem. B., 2009, 113, 23, 8026-8030. (d) B. Okesola, V. Vieira, D. Cornwell, N. Whitelaw, D. Smith, 1,3:2,4-Dibenzylidene-D-sorbitol (DBS) and its Derivatives-efficient, versatile and industriallyrelevant low-molecular-weight gelators with over 100 years of history and a bright future, Soft Matter., 2015, 11, 4768-4787.